The Meteoritical Society

Meteoritics & Planetary Science 44, Nr 10, 1407–1419 (2009)
Abstract available online at http://meteoritics.org

Extent of thermal ablation suffered by model organic microparticles during aerogel capture at hypervelocities

M. J. BURCHELL[1*], N. J. FOSTER[1], J. ORMOND-PROUT[2], D. DUPIN[2], and S. P. ARMES[2]

[1]School of Physical Sciences, Ingram Building, University of Kent, Canterbury, Kent CT2 7NH, UK
[2]Dainton Building, Department of Chemistry, University of Sheffield, Brook Hill, Sheffield, South Yorkshire S3 7HF, UK
[*]Corresponding author. E-mail: m.j.burchell@kent.ac.uk

(Received 27 April 2009; revision accepted 13 September 2009)

Abstract–New model organic microparticles are used to assess the thermal ablation that occurs during aerogel capture at speeds from 1 to 6 km s^{-1}. Commercial polystyrene particles (20 μm diameter) were coated with an ultrathin 20 nm overlayer of an organic conducting polymer, polypyrrole. This overlayer comprises only 0.8% by mass of the projectile but has a very strong Raman signature, hence its survival or destruction is a sensitive measure of the extent of chemical degradation suffered. After aerogel capture, microparticles were located via optical microscopy and their composition was analyzed in situ using Raman microscopy. The ultrathin polypyrrole overlayer survived essentially intact for impacts at ~1 km s^{-1}, but significant surface carbonization was found at 2 km s^{-1}, and major particle mass loss at ≥3 km s^{-1}. Particles impacting at ~6.1 km s^{-1} (the speed at which cometary dust was collected in the NASA Stardust mission) were reduced to approximately half their original diameter during aerogel capture (i.e., a mass loss of 84%). Thus significant thermal ablation occurs at speeds above a few km s^{-1}. This suggests that during the Stardust mission the thermal history of the terminal dust grains during capture in aerogel may be sufficient to cause significant processing or loss of organic materials. Further, while Raman D and G bands of carbon can be obtained from captured grains, they may well reflect the thermal processing during capture rather than the pre-impact particle's thermal history.

INTRODUCTION

It has long been established that fast-moving cosmic dust particles in space can be preserved by capture in aerogel targets (see Burchell et al. [2006] for a review). Since the first laboratory demonstration of capture in aerogel (Tsou et al. 1988) and test flights on the STS, aerogel collectors have been flown in space for extended periods on several missions, e.g., on the EuReCa satellite (Brownlee et al. 1994; Burchell et al. 1999a), the Mir space station (Hörz et al. 2000), the International Space Station (Neish et al. 2005) and more recently on the Stardust mission, which in 2004 flew past comet 81P/Wild 2 (Brownlee et al. 2004, 2006). Aerogel is a highly porous, optically transparent solid of ultra-low density. Thus when particles impinge on such targets at the hypervelocities typically encountered in space (>1 km s^{-1}), they are not subject to the extreme shock pressures (~10^1–10^2 GPa) generated during impacts on conventional high-density targets such as metals. Instead, the particles experience peak shock pressures of ~1 GPa (depending on aerogel density) and tunnel into the aerogel to form distinctive tracks (where particles are mechanically strong enough to survive the initial impact shock mostly intact they form long, carrot shaped tracks), rather than impact craters. The particle can often be located (semi-)intact at the end of its track, rather than being identified by post mortem analysis of its melted residues on a crater wall. However, even if (partial) fragmentation is avoided, the captured particles typically experience some degree of thermal ablation before coming to rest, which may well be evident in their subsequent chemical or spectroscopic analysis.

In 2004, the NASA Stardust spacecraft flew past comet 81P/Wild 2 at a relative velocity of 6.1 km s^{-1} (Brownlee et al. 2004, 2006). The spacecraft carried density gradient silica aerogel targets with nominal front face density ~5 kg m^{-3}, changing smoothly to ~50 kg m^{-3} over their 3 cm depth (Tsou et al. 2003), although there is some evidence that not all the aerogel had a density gradient (e.g., based on an analysis of 180 tracks, Burchell et al. 2009 suggested that the Stardust aerogel behaved as if it had a typical density of ~20 kg m^{-3}). The captured cometary dust grains were returned to Earth in 2006, and are now available for laboratory investigation.

Many comet 81P/Wild 2 dust particle analyses have already been published, e.g., elemental composition (Flynn et al. 2006), isotopic analyses (McKeegan et al. 2006), mineralogy (Zolensky et al. 2006) and organic analysis (Sandford et al. 2006; Keller et al. 2006) and many more papers are now appearing (e.g., *MAPS* vol. 43(1/2) 2008, published 24 papers concerning Stardust); for a recent review see Burchell and Kearsley (2009). However, relatively few papers directly address the possible influence of thermal ablation during capture, and those that do are mostly focused on mineralogical changes (e.g., Noguchi et al. 2007; Roskosz et al. 2008) or fragmentation of particles due to mechanical effects (e.g., Trigo-Rodríguez et al. 2008). In particular, quantification of the possible loss or alteration of any organics that may be present in comet 81P/Wild 2 dust due to impact processing has been relatively neglected. Some detailed quantitative analyses of the organic contents of Wild 2 dust grains are now available, e.g., Cody et al. (2008). However, while these measurements are clear, the effect of the high velocity capture still remains to be fully determined.

It is known that hypervelocity capture, even in low density aerogels, can significantly alter the size and structure of the impinging projectile and thus potentially bias any subsequent analysis. For example, Bunch et al. (1991) show the presence of rims formed on particles during capture in aerogel, and Burchell et al. (2001) found significant reductions in diameter (by up to 20%) and hence mass (almost half the original mass in the worst case) for soda lime glass projectiles impacting aerogels of density 60 kg m^{-3} at 6 km s^{-1}. More recently, Noguchi et al. (2007) conducted laboratory-based studies of impacts using aerogel targets of density 30 kg m^{-3}; the mineralogical changes experienced by projectiles captured at 6.18 km s^{-1} indicated that their surface temperatures exceeded 500 °C for at least 1 μs. Similarly, Burchell et al. (2009) showed that 500 μm stainless steel projectiles captured in 30 kg m^{-3} aerogels at 5 km s^{-1} underwent melting (suggesting surface temperatures greater than 1400 °C) with significant ablation on their leading face. In addition, Hörz et al. (2008, 2009) reported that 60 μm alumina (Al_2O_3) particles fired into 20 kg m^{-3} aerogel at 6 km s^{-1}, underwent both ablation and melting, indicating surface temperatures of more than 2054 °C. Our analysis of the Hörz et al. data (based on the images presented in their papers) suggests that up to 25% of the original projectile mass was lost during aerogel capture. Separately, Roskosz et al. 2008, suggest that particle fragments shed along the track during capture and mixed with molten aerogel may have experienced elevated temperatures (of the order of 2000 K) for time periods of up to 0.1 msec.

Such thermal damage can cause substantial mineral processing within the projectile interior over length scales of (at least) several micrometers, which poses significant problems for reliable post mortem analyses of aerogel-captured dust grains. Individual particles with final diameters of tens of micrometers can be extracted and cross-sectioned in order to expose their pristine interior (e.g., see Bunch et al. 1991), thus enabling their original structure to be determined. However, the (near-)surface structure of such dust grains (and indeed the interiors of micrometer-sized grains and smaller) will be invariably compromised and any volatile components may be preferentially liberated, thus altering their apparent elemental composition. Organic dust grains are undoubtedly even more sensitive to thermal ablation during aerogel capture than their mineralogical and metallic counterparts, since their thermal decomposition temperatures are typically much lower.

The aerogel capture of model organic particles has been the subject of a few prior studies. For example, Burchell et al. (2004) showed that poly(ethyl methacrylate) and poly(methyl methacrylate) particles (of 130 μm and 187 μm diameter, respectively after capture) both gave recognizable Raman signals after their capture within a 60 kg m^{-3} aerogel at 5 km s^{-1}. This suggested that the surface properties of these projectiles had not altered significantly, which is perhaps surprising given the relatively low thermal decomposition temperatures of these two aliphatic polymers (~550–600 K). Unfortunately, the highly polydisperse nature of these projectiles meant that their original diameters could not be compared with their post-impact diameters, thus it was not possible to examine whether any mass loss occurred during their aerogel capture. In parallel to this, Burchell et al. (2006b) reported the observation of highly distinctive D and G Raman bands (which are characteristic of amorphous carbon) in organic-rich meteorites fired into aerogel. In principle, the position and width of these bands can be used to determine the degree of order of the samples. However, Foster et al. (2007) showed that these two bands were sensitive to shifts in their peak positions and widths during capture. Since the peak positions and widths of the G bands are often used to indicate the degree of thermal metamorphism and crystalline ordering of a sample (e.g., Sandford et al. 2006 with regard to Stardust organic analysis), any modification during capture is a potential bias. Separately, detailed studies of the organic content of residues along track walls and in terminal grains from projectiles of known organic structure (e.g., coals, cocoa powder and fragments of Allende meteorite) have been carried out using two step laser-desorption laser-ionization mass spectrometry (Spencer et al. 2009), where it was found that deposits in track walls do not retain their original organic structure (with selective loss of different organic structures), whereas compounds in the terminal grains at the end of tracks may retain their original structure.

The aim of the present study was to use polypyrrole-coated 20 μm polystyrene microparticles as model projectiles for understanding the extent of thermal ablation that may occur during aerogel capture of micrometer-sized organic grains. Various syntheses of somewhat smaller conducting polymer-based particles (<2 μm diameter) were reported some years ago. These latter particles were used as model projectiles for mimicking the behavior of cosmic dust in

hypervelocity experiments involving an electrostatic Van der Graaff accelerator, since their electrical conductivity was sufficiently high to allow the efficient accumulation of surface charge (e.g., Keaton et al. 1990; Burchell et al. 1999b, 2002; Goldsworthy et al. 2004; Fujii et al. 2006). However, the electrically conductive nature of the polypyrrole overlayer is merely incidental in the present study, since acceleration was achieved using a light gas gun. This latter technique permitted the use of larger particles than previously because electrostatic accelerators have a strong inverse mass-velocity relationship for the projectiles, which, for speeds in excess of 1 km s^{-1}, typically requires particles of sub-micrometer dimensions, whilst light gas guns can directly fire a wide range of grain sizes. The important characteristics of our new model organic projectiles are three-fold: (i) the highly conjugated nature of the polypyrrole chains (which ensures a strong, highly distinctive spectroscopic signature due to a resonance Raman effect, Ormond-Prout et al. 2009); (ii) the ability to deposit this polypyrrole as a uniform, ultrathin overlayer onto 20 μm polystyrene latex; (iii) they are near-monodisperse, with a mean diameter of ~20 μm. Projectiles of this size can be readily identified by optical microscopy after capture within the aerogel, while Raman microscopy can be used to evaluate whether the polypyrrole overlayer has remained intact, or whether it has suffered chemical degradation. Thus the ultrathin nature of the polypyrrole overlayer ensures that such "core-shell" microparticles are highly sensitive to the onset of thermal ablation. Finally, if thermal ablation had indeed occurred, optical imaging of the captured particles coupled with their relatively narrow particle size distribution allows their approximate reduction in size (and hence mass loss) to be estimated. Whilst no one type of organic projectile can fully represent all organics in a study of impact processing, this work serves as a first step in development of a more general understanding of impact processing of organic materials during high-speed capture.

SAMPLES AND METHOD

Micro-Particle Preparation

Materials

Polystyrene microparticles with a mean diameter of 20 μm were purchased from Microbeads (Norway; http://www.micro-beads.com/Company.aspx accessed April 2009). Sodium 4-toluenesulfonate (95%) and $FeCl_3 \cdot 6H_2O$ were both purchased from Aldrich and used as received. De-ionized water (pH 6) was used for both polymerizations and subsequent purification, while methanol was obtained from Fisher Scientific. Pyrrole (Aldrich) was purified by alumina chromatography prior to use.

Polypyrrole Bulk Powder Preparation

$FeCl_3 \cdot 6H_2O$ (9.10 g) was dissolved in de-ionized water (100 ml) in a 125 ml jar. The solution was stirred using a magnetic stirrer bar. Sodium 4-toluenesulfonate (9.10 g) was then added to the jar and pyrrole monomer (1.0 ml) was added to the reaction mixture using a 1.0 ml syringe. The polymerization was stirred overnight at room temperature and the resulting black precipitate was isolated by vacuum filtration. The precipitate was washed several times with de-ionized water and then with methanol. The purified black powder was dried in a 50 °C oven overnight. The yield of polypyrrole bulk powder was approximately 90%.

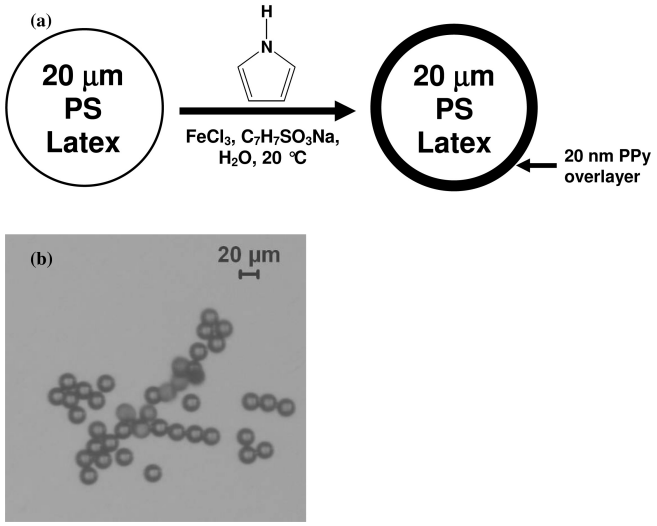

Fig. 1. a) Reaction scheme for the in situ deposition of polypyrrole onto 20 μm polystyrene microparticles from aqueous solution containing sodium tosylate ($C_7H_7SO_3Na$) at 20 °C. b) Optical image of the polypyrrole-coated polystyrene microparticles.

Polypyrrole Coating of the Polystyrene Microparticles

Lascelles and Armes (1995; 1997) have previously described the synthesis of polypyrrole-coated polystyrene microparticles with a mean diameter of 1–2 μm. Recently, this work has been extended to include polypyrrole-coated poly(methyl methacrylate) latexes ranging in size from 1.19 to 30 μm (Ormond-Prout et al. 2009). A similar coating protocol was utilized in the present study for the 20 μm polystyrene micro-particles (see Fig. 1a).

Sodium 4-toluenesulfonate (0.6317 g) and $FeCl_3 \cdot 6H_2O$ (0.6317 g) were dissolved in deionized water (90 ml) in a 125 ml jar. Polystyrene microparticles (10.0 g) were then added to this stirred reaction solution, and pyrrole monomer (69.5 μl; corresponding to a polypyrrole mass loading of 0.80%, or a mean overlayer thickness of 19 nm) was added to the reaction mixture using a micropipette. The polymerization was allowed to proceed for 24 h at room temperature. The black dispersion was then filtered under gravity and the coated particles were purified by three centrifugation-dispersion cycles (3,000 rpm for 20 minutes). After each centrifugation cycle, the supernatant was carefully decanted and the sedimented particles were redispersed in de-ionized water. This protocol removed the spent oxidant and traces of

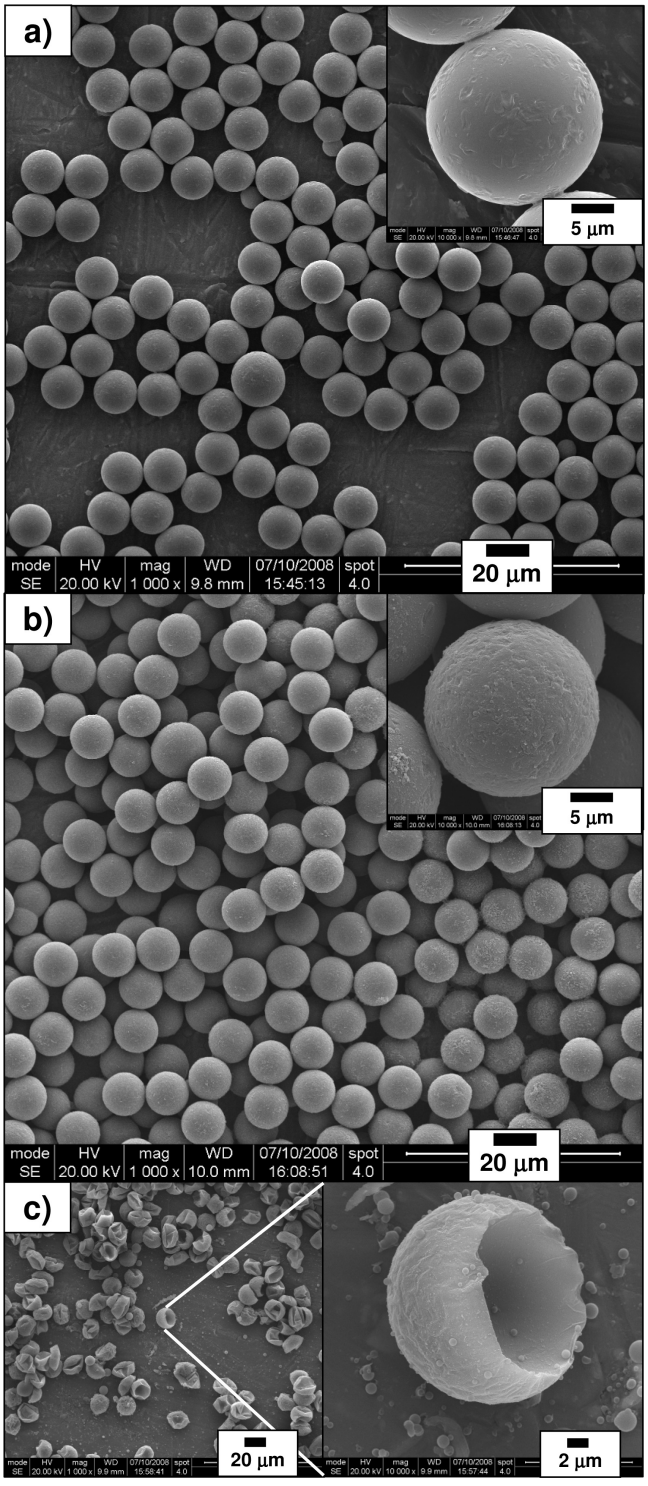

Fig. 2. SEM images of a) uncoated 20 μm polystyrene microparticles, b) polypyrrole-coated 20 μm polystyrene microparticles before solvent extraction, c) polypyrrole residues after solvent extraction of polypyrrole-coated 20 μm polystyrene microparticles for 24 h at 20 °C. The "goldfish bowl" morphology obtained for the insoluble polypyrrole residues that remain after solvent extraction confirms the "core-shell" morphology of the original microparticles.

unreacted pyrrole monomer. The purified polypyrrole-coated polystyrene microparticles were dried in an oven at 50 °C overnight to obtain a free-flowing grey powder (see the optical micrograph shown in Fig. 1b).

The scanning electron micrograph of the pristine polystyrene microparticles shown in Fig. 2a confirms their spherical morphology, narrow size distribution and smooth, relatively featureless surface morphology. An image of the polypyrrole-coated polystyrene microparticles is shown in Fig. 2b. The conducting polymer overlayer is relatively smooth and featureless at this magnification, as expected. The well-defined "core-shell" nature of these polypyrrole-coated polystyrene microparticles was verified by solvent extraction of the underlying linear polystyrene chains using THF for 24 h at 20 °C. An image of the resulting insoluble polypyrrole residues in the form of "broken egg-shells," or "goldfish bowls," is shown in Fig. 2c: this post-mortem analysis confirms the contiguous nature of the polypyrrole coating. Close inspection at high magnification suggests that the polypyrrole overlayer thickness is approximately 20 nm, which is very close to that originally targeted.

Assuming that the polypyrrole overlayer is indeed both smooth and uniform, the mean polypyrrole overlayer thickness can be calculated given the mean radius of the polystyrene microparticles, the densities of polystyrene and polypyrrole and the mass fractions of these two polymers (Lascelles and Armes 1997). Helium pycnometry (using a Micromeritics 1330 AccuPyc instrument) was used to measure the solid-state densities of the polystyrene latex and the polypyrrole bulk powder as 1.05 and 1.46 g cm^{-3}, respectively (in good agreement with the literature values). Thus the calculated polypyrrole overlayer thickness was 20 ± 1 nm.

Aerogel Targets

The silica aerogel used in this work had a density of between 25 and 35 kg m^{-3} (measured separately for each block). The aerogels were from the same batch as those described in Burchell et al. (2009). They were originally 10 cm long, with a cross section of 3 cm × 3 cm, but were cut into 4 cm lengths for these experiments.

Analysis Facilities

Various analytical techniques were used to characterize the uncoated and polypyrrole-coated polystyrene microparticles reported in this paper. Optical microscopy of the uncoated polystyrene latex was achieved using a James Swift MP3502 (Prior Scientific Instruments Ltd.) microscope equipped with a Nikon Coolpix 4500 digital camera. After coating with an ultrathin polypyrrole overlayer, the microparticles were imaged (Fig. 1b) using a Leica MZ16 stereo microscope equipped with a Leica DFC420 camera. The latter was also used to image particles after their capture within aerogel targets. Scanning electron microscopy (SEM)

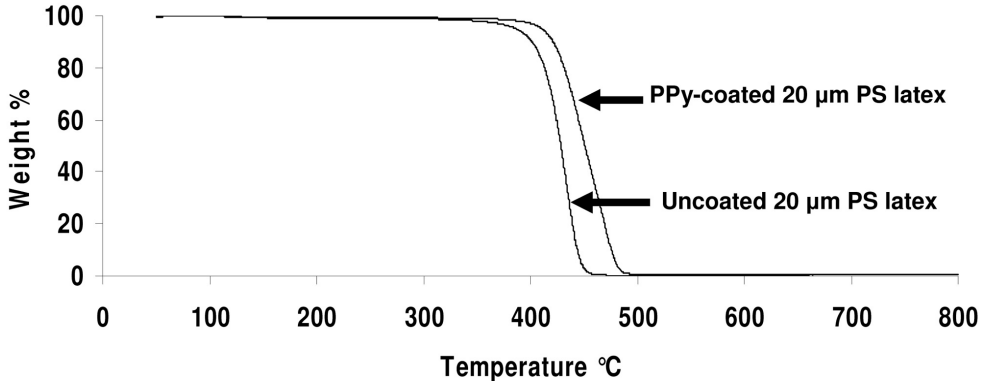

Fig. 3. Thermogravimetric analysis curves obtained under nitrogen for the uncoated 20 µm polystyrene microparticles and the polypyrrole-coated 20 µm polystyrene microparticles. The polypyrrole overlayer appears to confer slightly enhanced thermal stability, with the coated microparticles only showing signs of mass loss from 400 °C upwards. These curves indicate the minimum temperature required to cause significant mass loss from the microparticles used in this study.

images of the microparticles were obtained using a FEI Inspect instrument operating at 5 kV. All samples were sputter-coated with thin gold overlayers prior to SEM imaging to prevent sample-charging effects.

Particle size distributions for the uncoated and polypyrrole-coated polystyrene microparticles were also obtained by laser diffraction. A Malvern Mastersizer 2000 instrument equipped with a small volume (about 50 mL) Hydro 2000SM sample dispersion unit, a HeNe laser operating at 633 nm and solid-state blue laser operating at 466 nm, was employed for these measurements. The stirring rate was adjusted to 1,500 rpm. Corrections were made for background electrical noise and laser scattering due to contaminants on the optics and within the samples. Both the polypyrrole-coated and the uncoated polystyrene microparticles were analyzed five times and the data were averaged. Typical analysis times were two minutes per sample after alignment and background measurements. The raw data were analyzed using Malvern software. The volume-average mean diameter, $D_{4/3}$, is mathematically expressed as $D_{4/3} = \Sigma\ D_i^4 N_i\ /\ \Sigma\ D_i^3 N_i$. The standard deviation for each diameter provides an indication of the width of the distribution. After each measurement, the cell was rinsed three times with ethanol, followed by three times with doubly-distilled water. The glass walls of the cell were carefully wiped with lens cleaning tissue to avoid cross-contamination and the laser was aligned centrally on the detector.

Thermogravimetric analysis (TGA) was conducted using a Perkin-Elmer Pyris 1 TGA instrument, which monitors the change in mass with increasing temperature. Dried samples were heated up to 800 °C in nitrogen at a heating rate of 20 °C min^{-1}. The software was programmed to heat the samples to 50 °C for one minute to remove any traces of moisture prior to each run. In some cases the grey-black char that remained at the end of the heating run was later analyzed by Raman microscopy. The TGA results are shown in Fig. 3, indicating that for the coated micro-particles a purely temperature related mass loss occurs from 400 °C upwards.

X-ray photoelectron spectroscopy (XPS) is an established surface analytical technique. It has a typical sampling depth of 2–10 nm, so it is well suited for the characterization of these polypyrrole-coated polystyrene microparticles (e.g., Perruchot et al. 1996; Ormond-Prout et al. 2009). In principle, the nitrogen atoms in the polypyrrole chains should act as a unique elemental marker for this component, since polystyrene contains no nitrogen. However, it is possible that there are nitrogen-based species at the surface of the pristine polystyrene latex, due to either polymeric stabilizers such as poly(*N*-vinylpyrrolidone), cationic surfactants or azo initiator fragments. Figure 4 depicts three XPS survey spectra recorded for an uncoated 20 µm polystyrene latex, polypyrrole bulk powder and the polypyrrole-coated 20 µm polystyrene latex. There is no detectable nitrogen signal for the pristine polystyrene latex, hence the polypyrrole surface coverage of the latex can be readily estimated by normalizing the N1s signal observed for the coated latex with respect to the N1s signal obtained for the polypyrrole bulk powder. This approach yields an estimated polypyrrole surface coverage of approximately 80%, based on comparing the N1s signal intensity for the polypyrrole-coated 20 µm polystyrene microparticles with that of the polypyrrole bulk powder.

Raman spectra of microparticles before and after their aerogel capture were recorded using a Yobin Yvon Raman microscope (HR640 spectrograph with a LN_2 cooled CCD and He-Ne laser illumination). The maximum laser power was 10 mW, the spot size on the sample was 3–5 µm (full width) and the dispersion was 0.5 cm^{-1} at the CCD. A series of attenuation filters were used to reduce the laser power (8% of full power was typically used) to minimize sample heating due to the laser illumination. Typical accumulation times ranged from 12–14 and 28–56 min per spectrum in total (for raw particles and those captured in aerogel, respectively),

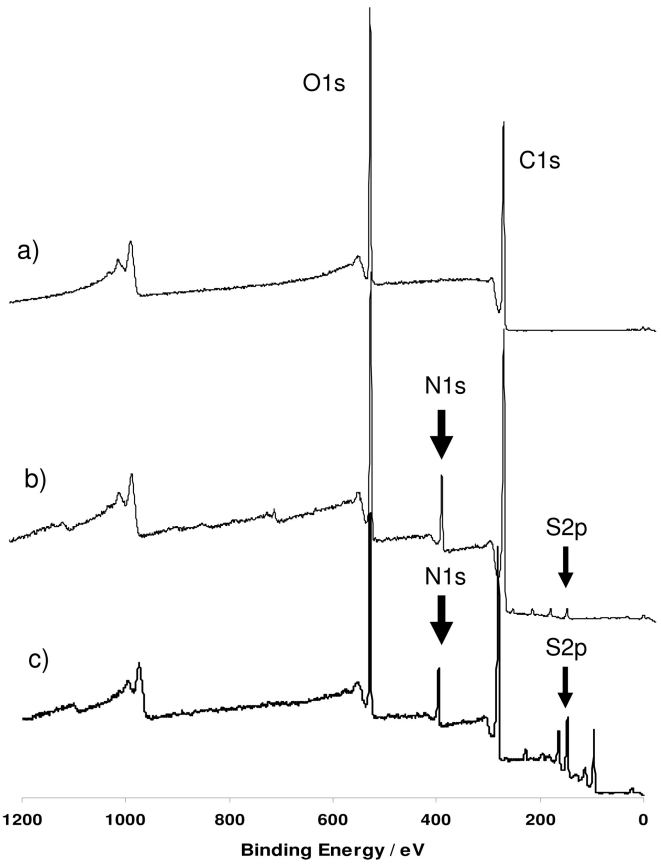

Fig. 4. XPS survey spectra for a) uncoated 20 μm polystyrene microparticles, b) 20 μm polystyrene microparticles coated with 20 nm polypyrrole, c) polypyrrole bulk powder.

where each full spectrum (ranging from 200 to 4000 cm^{-1}) was constructed by joining several sub-spectra taken in more limited wave shift number ranges.

Light Gas Gun Experiments

A two-stage light gas gun at the University of Kent (Burchell et al. 1999c) was used to fire buckshot-like clouds of projectiles at the aerogel targets; thus multiple impacts were achieved for each shot at near-equal speeds. The speed was varied by controlling the nature of the light gas used (e.g., sulfur hexafluoride, nitrogen or hydrogen) and was measured for each shot using a combination of laser light curtains and impact sensors on stop plates along the range of the gun (accurate to ±2%). The target chamber was evacuated to approximately 50 Pa in each shot. The projectiles were the polypyrrole-coated 20 μm polystyrene microparticles mixed with larger 50 μm diameter monodisperse glass beads. This was in order to increase the yield of small particles reaching the target. The glass beads were easily distinguishable from the organic projectiles within the aerogel, as the former gave much longer tracks that contained relatively large particles. Five different speeds (1.07, 1.95, 3.33, 4.55, and 6.11 km s^{-1}) were used in these experiments, with the latter corresponding to that experienced by the Stardust spacecraft. Examples of typical carrot tracks and aerogel-captured microparticles are shown in Figs. 5 and 6.

RESULTS AND DISCUSSION

Both the dried uncoated and polypyrrole-coated polystyrene microparticles are readily redispersed in water with the aid of an ultrasonic bath. These aqueous suspensions were diluted and analyzed using the laser diffraction method above. The particle size distributions obtained for the coated and uncoated microparticles are virtually indistinguishable, both yielding volume-average diameters of approximately 21.5 μm. Thus the polypyrrole overlayer does not cause any significant aggregation of the polystyrene microparticles. This result also suggests that individual microparticles (rather than aggregates) are likely to be fired as discrete projectiles in light gas gun experiments.

The particles were also examined by optical microscopy prior to the light gas gun experiments. The mean number-average diameter of the polypyrrole-coated microparticles was 20.1 ± 1.2 μm, which is comparable to that obtained from the laser diffraction measurements. The individual microparticles captured within the aerogel were sized in situ by optical microscopy; 8 microparticles were measured at 1.07 km s^{-1}, 5 at 1.95 km s^{-1}, 7 at 3.33 km s^{-1}, 5 at 4.55 km s^{-1} and 3 at 6.11 km s^{-1} (see Table 1 and Fig. 7). At the lowest impact speeds, the captured microparticles had comparable dimensions to the original pristine microparticles, which confirmed that no significant mass loss had occurred. However, there was a mean reduction in diameter of 3 μm (15%) at 3.3 km s^{-1}, which is more than sufficient to remove the 20 nm polypyrrole coating. More substantial mass losses were observed at higher impact speeds. At 6.11 km s^{-1} (which is similar to that at which cometary dust was collected by Stardust), the captured particles had only 54% of the original particle diameter, which is equivalent to an 84% mass loss.

Raman spectra were recorded for the pristine 20 μm polystyrene latex, polypyrrole bulk powder and polypyrrole-coated 20 μm polystyrene latex (see Fig. 8). These spectra were baseline-corrected and scaled by a multiplying factor to aid comparison. The 20 μm polystyrene latex spectrum in Fig. 8 was scaled to match the intensity of the band at 3055 cm^{-1} in the polypyrrole-coated 20 μm polystyrene latex spectrum, while the polypyrrole bulk powder spectrum was scaled to match the 935 cm^{-1} band in the polypyrrole-coated 20 μm polystyrene latex spectrum. Band positions and peak widths are summarized in Table 2. The Raman spectra obtained for the uncoated 20 μm polystyrene latex and the polypyrrole bulk powder are in very good agreement with the literature spectra (Table 3). For polystyrene, we refer to the ASTM E 1840 standard used to calibrate Raman spectrometers. The polystyrene latex bands (and their relative intensities) correlate very well with those observed for the reference standard. For polypyrrole, there is a wide range of

Fig. 5. Example track in aerogel for impact of 20 µm polystyrene microparticles coated with 20 nm polypyrrole at an impact speed of 1.07 km s^{-1} (the impact was from the right). A whole track is shown, with a total length of 1088 µm. The front face of the aerogel appears as a near-vertical line near the right-hand side of the image. The track is the faint, tapering cylinder across the middle of the image and the captured particle (marked with an arrow) is in the left of the image at the end of the track.

literature available (e.g., Oddi et al. 1986; Inoue et al. 1987; Liu 2004; Chuang et al. 2005); in Table 3 we refer to band assignments from Liu (2004), who, using a He-Ne laser as here, reported that Raman spectral features obtained using surface-enhanced Raman spectroscopy varied according to the electrical conductivity of the polypyrrole. Again, there is generally good agreement between our spectra and these literature spectra. As well as relatively narrow peaks, Raman spectra recorded for polypyrrole usually exhibit a broad spectral region from 1000–1600 cm^{-1}, which is also observed here.

Despite its very low conducting polymer mass loading (<1%), the Raman spectrum of the polypyrrole-coated polystyrene latex is clearly dominated by this minor component. All the major features assigned to polypyrrole (e.g., counter-ions, N-H deformation, ring stretching and C = C bond stretching) are observed. In addition, several features due to the underlying polystyrene latex are also visible, e.g., the aromatic C-H out-of-plane bending mode at 1002 cm^{-1} and the aromatic and aliphatic C-H stretches just above and below 3000 cm^{-1}, which are not found in the polypyrrole bulk powder spectrum.

Similar Raman observations of polypyrrole have been reported for micrometer-sized polypyrrole-coated polystyrene latexes using a 1.06 µm laser source, although at this longer wavelength no features due to the underlying polystyrene were detected (Lascelles et al. 1997; Cairns 1999). In both cases, this remarkable enhancement is due to a resonance Raman effect caused by the strongly absorbing nature of the highly conjugated polypyrrole chains. In essence, this means that Raman spectroscopy is unusually sensitive to the surface composition of these core-shell latexes. Coupled with the excellent spatial resolution offered by Raman microscopy (~1 × 1 μm^2) and the ultrathin nature of the conducting polymer overlayer, this spectroscopic phenomenon offers a potentially decisive advantage for the in situ interrogation of individual latex particles.

Raman spectra recorded in situ for individual aerogel-captured microparticles are shown in Fig. 9. Inevitably, the typically signal-to-noise in these spectra is significantly worse than that observed for spectra recorded from macroscopic samples (see Fig. 8), even though spectral accumulation times were increased, typically by a factor of 4. This limitation is due to two factors: (i) constraints imposed by the microscopic sample volume and (ii) unwanted light scattering by the aerogel matrix. At 1.17 km s^{-1}, the Raman spectrum of the aerogel-captured microparticle (Fig. 9a) is very similar to that observed for the original polypyrrole-coated polystyrene latex; bands attributable to both the polypyrrole coating and the polystyrene core are observed. Given the ultrathin nature of the polypyrrole coating, this suggests that little or no thermal ablation has occurred under these conditions. This conclusion is consistent with particle size measurements made by optical microscopy (accurate to within ±1 µm), which confirms that the particles were captured intact (Fig. 7).

In contrast, all spectral features characteristic of both polypyrrole and polystyrene disappear after aerogel capture at 1.95 km s^{-1}. Instead, only two broad bands are seen (weakly) at 1374 and 1590 cm^{-1}; these are the carbon D and G bands. At 3.3 km s^{-1} (Fig. 8b), these bands are also observed (but more strongly). Similar observations were made for micro-particles captured at 6.17 km s^{-1}, (Fig. 9c) with an extra much broader band also observed at 2600 cm^{-1}. Optical microscopy studies indicate that no significant mass loss occurred at 1.95 km s^{-1}, with increasing mass loss apparent for impact speeds of 3.33 km s^{-1} and above (see Fig. 7). Thus, the ultrathin polypyrrole coating may or may not have been removed during impact, but the surface of the projectile has certainly been carbonized. At the higher speeds, the mass losses clearly correspond to substantial reductions in the particle dimensions, i.e., relatively thick layers are ablated that are much greater than the dimensions of the original 20 nm polypyrrole coating. Thus it is perfectly understandable that the polypyrrole spectral signature is no longer observed at

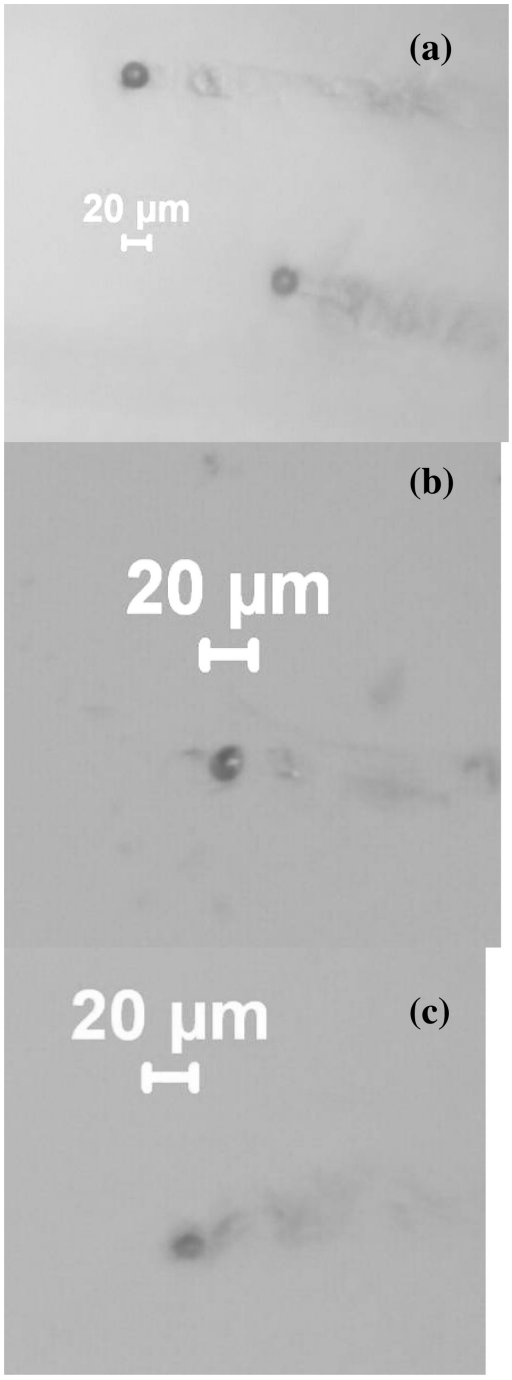

Fig. 6. Example particles captured at the ends of tracks in aerogel for impacts of 20 µm polystyrene microparticles coated with 20 nm polypyrrole at impact speeds of a) 1.17, b) 3.33, and c) 6.11 km s^{-1}. In all cases impacts were from the right.

higher speeds. However, what is surprising is that there is no longer any evidence for the underlying polystyrene latex. This indicates that the final exposed surfaces of these organic micro-particles after capture must undergo substantial thermal processing, i.e., not only has a surface layer been ablated but the newly-exposed surface has also been heated.

Table 1. Particle diameters after capture in aerogel.

Impact speed (km s^{-1})	Average particle diameter after capture (µm)	% size surviving capture	% mass surviving capture
1.07	20.5 ± 0.9	102 ± 8	~100
1.95	22.0 ± 3.4	109 ± 17	~100
3.33	17.1 ± 3.8	85 ± 20	61
4.55	15.9 ± 3.2	79 ± 16	49
6.11	10.9 ± 1.0	54 ± 6	16

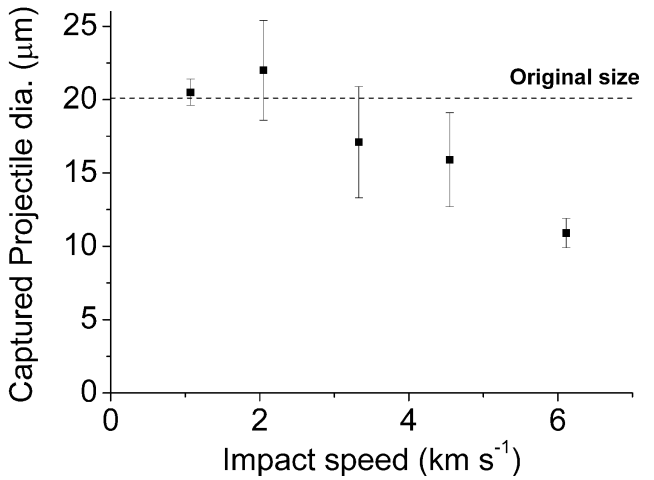

Fig. 7. Effect of varying the impact speed on the mean diameter of the aerogel-captured particles. The mean diameter (and 1σ spread of data) is shown at each impact speed. Also shown (dashed line) is the mean pre-impact diameter. Above 2 km s^{-1} the mean captured particle diameter starts to fall significantly below the pre-impact diameter.

The new band at 2000 to 3000 cm^{-1} in the high-speed capture events is unexplained. Raman spectra were recorded for the pristine 20 µm PS latex and PPy bulk powder after pyrolysis by thermogravimetry under nitrogen, but neither sample produced this spectral feature.

The Raman bands observed at 1327–1374 cm^{-1} and 1587–1590 cm^{-1} in impacts at 1.95 km s^{-1} and above are typical of the well-known D and G bands, respectively, that have been reported for amorphous carbon. Based on the width and position of the G band, the data obtained at 6.17 km s^{-1} are at the lower end of the range of values reported for cometary dust grains captured in the Stardust aerogel collector (Sandford et al. 2006; Rotundi et al. 2008). Similarly, the D and G band widths lie just within the range reported by Rotundi et al. (2008) for Stardust cometary grains. In the Stardust analyses, the positions and widths of the D and G bands were used to assess the degree of (dis)order of the carbonaceous residues in 81P/Wild 2 dust grains and make a comparison with meteorites and interplanetary dust particles (although it should be noted that Foster et al. 2007 showed that capture alters both the peak positions and width of these D and G bands). However, we emphasize that our present study (and that of Foster et al.

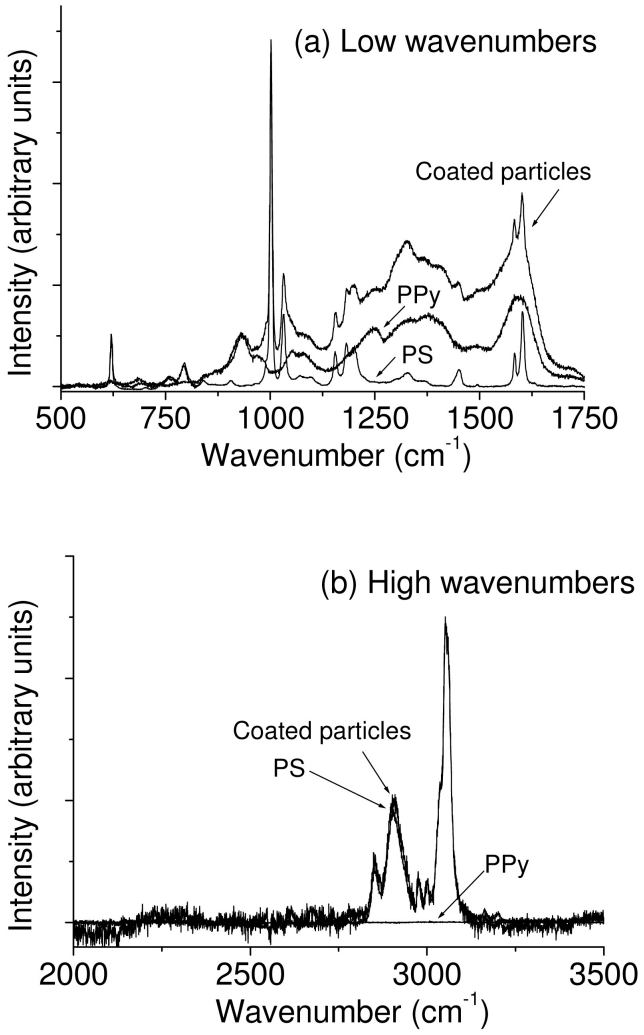

Fig. 8. Raman spectra recorded for uncoated 20 μm polystyrene microparticles ("PS"), polypyrrole bulk powder ("PPy") and polypyrrole-coated 20 μm polystyrene microparticles ("Coated particles") at a) low and b) high wavenumbers. All spectra have had the baseline set to zero. In both (a) and (b) the "PS" and "PPy" spectra were scaled such that, at 3055 and 931 cm^{-1} respectively, they had the same intensity as the "Coated particles" spectrum. In (a) the "Coated particles" spectrum clearly contains the features of both "PS" and "PPy" in near-equal measure. In (b) the "PS" and "Coated particles" spectra agree so well it is difficult to separate them; the only major difference is that the "PS" spectrum shows smaller noise fluctuations and has a slightly lower intensity at 2908 cm^{-1}, whereas the "PPy" spectrum is distinct from that from the "Coated Particles", showing no evidence for any bands associated with aromatic bending and aliphatic C-H stretching.

2007) involves studying the surfaces of particles in situ, whereas that of Rotundi et al. 2008 involved analysis of both whole grains (after extraction from the aerogel) and microtomed thin-sections of grains extracted from the aerogel (i.e., a mixture of both surface and interiors of particles were studied). However, most of the samples studied by Rotundi et al. (2008) were whole grains, and, unlike here, 3 (out of 11) of

Table 2. Wavenumbers and full widths in each Raman spectrum. The three strongest bands in each spectrum are in italics.

Sample	Peak wavenumber (width) cm^{-1}
20 μm polystyrene microparticles	621 (4), 794 (30), *1002 (6)*, 1032 (9), 1156 (11), 1181 (8), 1198 (27), 1325 (54), 1449 (27), 1591 (26), *1603 (13)*, 2851 (10), 2907 (48), *3055 (27)*
Polypyrrole bulk powder	*618 (33)*, 688 (38), 878 (107), *935 (39)*, 977 (29), 1069 (80), 1238 (101), 1319 (143), 1384 (163), *1593 (72)*
Polypyrrole-coated polystyrene particles	621 (6), 793 (10), 931 (50), *1002 (6)*, 1034 (11), 1137 (103), 1322 (100), 1559 (70), *1601 (56)*, 2851 (14), 2908 (61), *3055 (27)*

Table 3. Wavenumbers for major Raman bands taken from literature spectra.

Sample	Wavenumber (cm^{-1})
Polystyrene: (ASTM E 1840)	620.9, 795.8, 1001.4, 1031.8, 1155.3, 1450.5, 1583.1, 1602.3, 2852.4, 2904.5, 3054.3
Polypyrrole: (Liu 2004)	918–932 (counter anions), 1042–1053 and 1082–1083 (N-H in-plane deformation), 1329–1333 and 1377–1412 (ring stretching), 1599–1613 (C = C bond stretching).

these grains showed not just carbon D and G bands, but also bands at ~2900 cm^{-1}, which are characteristic of aliphatic C-H stretches. Thus whilst here the bands at higher wavenumbers were also lost at 6 km s^{-1}, it appears that such bands can in at least some cases survive aerogel capture.

The incident mean kinetic energy, KE, ($1/2\ mv^2$), of the micro-particles in our light gas gun experiments is relatively well-defined, since the particle mass and speed are highly constrained in each shot. Thus the maximum energy available for thermal ablation during an impact is readily calculated. However, in practice only some fraction *f* of this KE is involved in heating the micro-particles, since there are energy losses due to radiation and in heating the aerogel itself. Here we consider if the experimental mass losses place any constraints on *f*. In Fig. 10 the incident projectile kinetic energy (normalized to the molar mass of the particles which, to a good first approximation, comprise simply polystyrene) is shown vs. impact speed. The various curves for *f* indicate the available energy per mol if a specified fraction *f* of the kinetic energy is transferred as heat to the particle.

From Fig. 10 it can be seen that, at speeds of less than 2.5 km s^{-1}, even if all the kinetic energy is transferred to heat up the particle (i.e., if $f = 1.0$), this is insufficient to break any of the covalent chemical bonds in the polystyrene (if averaged over the whole particle, of course as discussed later, some bonds could be broken if the energy deposition were more localized). In reality, the kinetic energy will not be instantly converted into heat, since the particle takes some finite time, at least of the order of μs to lose its kinetic energy. During this time, heat conduction will not be able to transport the heat

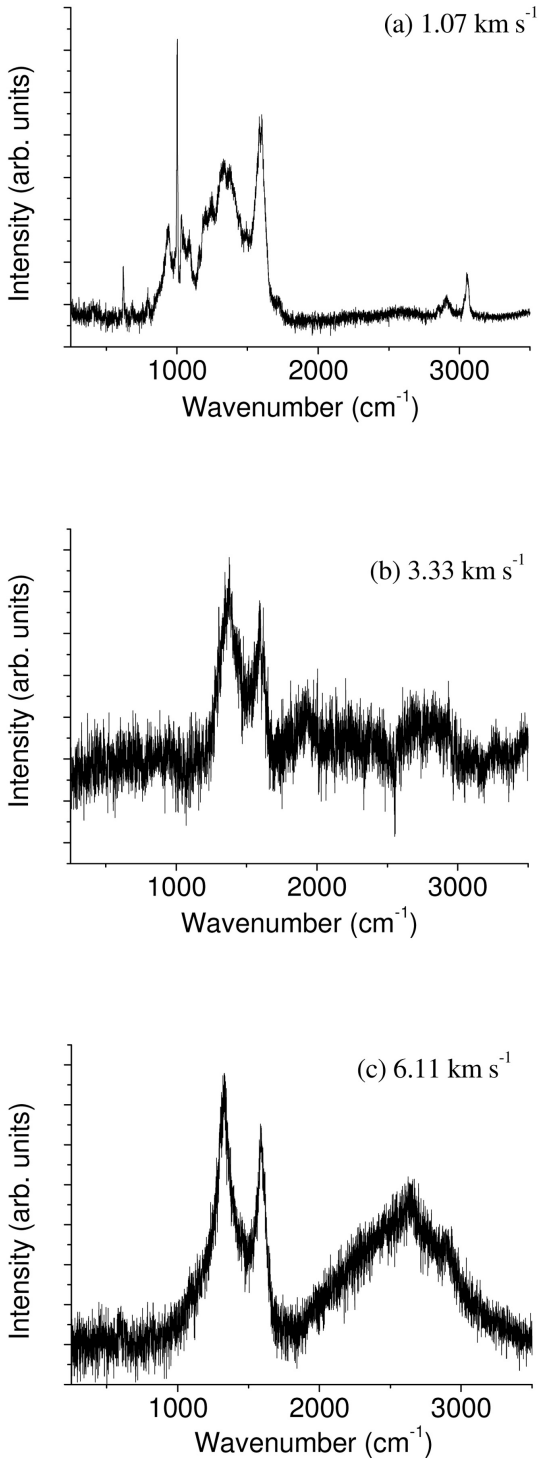

Fig. 9. Raman spectra recorded in situ for individual PPy-coated polystyrene microparticles captured in aerogel at impact speeds of: (a) 1.07 km s^{-1}, (b) 3.33 km s^{-1} and (c) 6.11 km s^{-1}. In (a) the spectrum resembles that of the pre-shot coated particles. However, in (b) and (c) the distinct peaks in (a) have been replaced by broad peaks at 1374 and 1590 cm^{-1}, which correspond to the distinctive carbon D and G bands due to amorphous carbon. Also evident in (c) (but not assigned) is a very broad feature centred at ~2758 cm^{-1}.

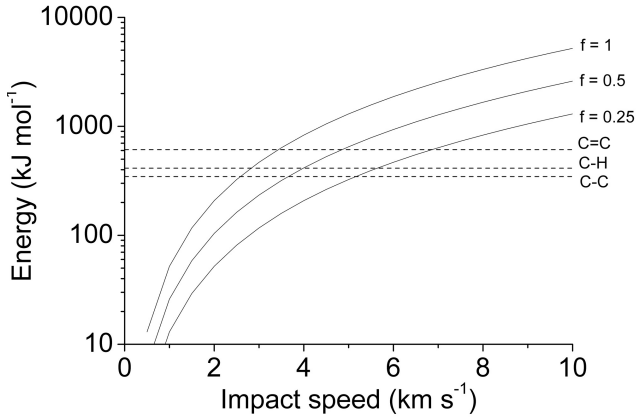

Fig. 10. Variation of incident kinetic energy per mol of projectile with impact speed. Solid curves assume that a fraction *f* of the energy is converted into heat and dissipated over the whole particle. Dashed (horizontal) lines are average bond energies taken from the literature for the three types of bonds (C-C, C-H and C = C) present in the polystyrene-based microparticles used in this study.

energy uniformly throughout the entire volume of the particle. In the absence of a validated model for deceleration of particles in aerogel and a lack of knowledge of the true value of *f*, we nevertheless make the following qualitative arguments.

First we note that cleavage of all chemical bonds in each styrene residue is difficult even at the highest speed used here. Each C_8H_8 styrene residue contains 3 × C-H aliphatic bonds, 5 × C-H aromatic bonds, 3 × C = C bonds and 5 × C-C bonds. Taking mean values for these bond energies implies that breaking all 16 bonds would require ~7100 kJ mol^{-1}. Even with $f = 1.0$ there is insufficient kinetic energy available to do this below impact speeds of 10 km s^{-1}. This partly explains why there are always residual particles found here within the aerogel even at impact speeds of 6.1 km s^{-1}.

We next consider selective cleavage of the bonds. Whilst the main chain C-C bond is the weakest bond, in high energy conditions multiple bond breaking is expected (e.g., see Gies et al. 2007). Indeed, previously, in impact ionization studies using similar polypyrrole-coated polystyrene latex particles, Goldsworthy et al. (2003) showed that impact-induced fragmentation gave rise to a strong signal due to the tropylium cation ($C_7H_7^+$; m/e = 91). The formation of this species involves cleavage of two C-C bonds (i.e., twice the mean bond energy of 346 kJ mol^{-1} = 692 kJ mol^{-1}). It is also noteworthy that, if this degradation mechanism also occurs during capture in aerogel targets (as distinct from impacts on solid metal targets), it would account for (i) the observation of amorphous carbon char (due to the development of conjugation along the residual aliphatic polyacetylenic backbone) and (ii) the substantial mass loss (due to loss of the volatile $C_7H_7^+$ species) observed at higher speeds. For example, if the C_8H_8 polystyrene repeat units were all converted into a $(CH)_x$-type amorphous carbon char, this would account for a very substantial mass loss (91/104 × 100

= 87.5%) from the projectile, while requiring minimal energy for bond cleavage.

If we accept this selective bond cleavage scenario and further assume that the eliminated mass was the only part of the particle that was heated, we can deduce the associated *f* value required to produce the minimal energy deposit needed. A single *f* value does not explain all the experimental data; the best fit being $f = 0.35$. Given our "minimum bound" assumptions that only the eliminated molecular fragments are heated and then only to the point necessary to cleave the C-C bonds, this implies that *f* must exceed the minimum value of 0.35.

CONCLUSIONS

Near-monodisperse 20 μm diameter polystyrene latex has been coated with a 20 nm contiguous overlayer of polypyrrole from aqueous solution. These new organic micro-particles have a well-defined "core-shell" morphology and a distinctive Raman spectral signature; as such, they are ideal model projectiles for mimicking the behavior of organic dust grains impinging on aerogel targets at hypervelocities. Moreover, the relatively narrow size distribution of these microparticles allowed their mass loss during aerogel capture to be estimated as their incident hypervelocity was systematically varied.

The polypyrrole-coated polystyrene micro-particles captured in aerogel at 1.07 km s^{-1} underwent no significant effects. Those captured at 1.95 km s^{-1} were not significantly ablated, but underwent surface processing (with loss of their distinctive Raman bands and appearance of weak, broad D and G bands due to amorphous carbon). Particles captured at 3.3 to 6.1 km s^{-1} were both thermally processed and substantially ablated during aerogel capture (mass losses of 39% and 84%, respectively), with the corresponding Raman spectra being dominated by D and G bands due to the production of amorphous carbon during impact (and whose positions and widths are compatible with those found in the Stardust Wild cometary dust samples). After aerogel capture at 6.1 km s^{-1} in our light gas gun experiments here the spectral signals in the range of 2800–3000 cm^{-1} (due to the aliphatic and aromatic C-H stretches in polystyrene) in the original micro-particles were lost, although there is evidence (Burchell et al. 2004; Rotundi et al. 2008) that this spectral feature can survive high speed aerogel capture.

Significant mass loss of these organic micro-particles was only found for impact speeds above 2 km s^{-1}, which based on TGA analysis suggests surface temperatures exceeded 400 °C at these speeds. Based on the degree of mass loss, and assuming a simple model for bond cleavage, we estimate that at least 35% of the incident kinetic energy was coupled back into the particles as heat during their aerogel capture.

These laboratory experiments have important implications for the interpretation of dust grains originating from comet 81P/Wild-2 captured in aerogel targets during the recent Stardust mission. Although polystyrene and polypyrrole are not necessarily appropriate analogues for all complex organic molecules, our results suggest that substantial thermal processing and chemical degradation of the surface of organic-rich cometary grains can be expected at a capture speed of 6.1 km s^{-1} (i.e., under Stardust capture conditions). Furthermore, ablation is not merely confined to surface degradation, but can involve reductions in grain diameters of the order of micrometers (based on a heat pulse of the order of 1 μs). Thus the search for genuine primordial organic matter within cometary dust grains captured by Stardust aerogels will most likely require microtomy of relatively large (tens of micrometers) terminal grains, with careful examination of the grain interior well away from both edges and fracture features. Moreover, any organic debris shed during aerogel capture and embedded in the aerogel walls of the carrot tracks is also likely to be unrepresentative of the original cometary dust grains, since it will have typically experienced significant heating during capture. To reduce such problems with collection of organic-rich micro-particles in space, any future mission using low density aerogels should aim to minimize the collection speed, ideally to 1 km s^{-1} or less.

However, several caveats should be added to these conclusions. Firstly, not all organic materials will have the same thermal decomposition temperatures as here. Also, the 20 μm diameter projectiles used here are at the large end of the size range found in Stardust samples. Further, the survival of organic materials found as sub-micrometer sub-grains in larger particles of mixed organic-mineral content has not been examined. Finally, we note that the work here has focussed on the organic history of the projectiles, the aerogel itself may have an organic content, and at the track temperatures indicated here this may also undergo processing and complicate any subsequent organic analysis (Spencer and Zare 2007). This is a similar problem to that of some aspects of more general analysis in Stardust aerogels, e.g., the presence of GEMS (glass with embedded metal and sulfides) which, whilst possibly present in the cometary dust are also created as impact artefacts during capture in aerogel (Ishii et al. 2008).

Acknowledgments—MJB acknowledges support from STFC. SPA is the recipient of a five-year Royal Society/Wolfson Research Merit Award. NJF acknowledges support from the University of Kent alumni. D. D. is supported by an EPSRC Platform Grant (EP/E012949/1).

Editorial Handling—Dr. John Bradley

REFERENCES

Brownlee D. E., Hörz F., Hrubsch L., McDonnell J. A. M., Tsou P., and Williams J. 1994. Eureka!! Aerogel capture of micrometeoroids in space (abstract). 25th Lunar and Planetary Science Conference. pp. 183–184.

Brownlee D. E., Hörz F., Newburn R. L., Zolensky M., Duxbury T. C., Sandford S., Sekanina Z., Tsou P., Hanner M. S., Clark B. C., Green S. F., and Kissel J. 2004. Surface of young Jupiter family comet 81P/Wild 2: View from the Stardust spacecraft. *Science* 304:1764–1769.

Brownlee D., Tsou P., Aléon J., Alexander C. M. O'D., Araki T., Bajt S., Baratta G. A., Bastien R., Bland P., Bleuet P., Borg J., Bradley J.P., Brearley A., Brenker F., Brennan S., Bridges J. C. Browning N., Brucato J. R., Brucato H., Bullock E., Burchell M. J., Busemann H., Butterworth A., Chaussidon M., Cheuvront A., Chi M., Cintala M. J, Clark B. C., Clemett S. J., Cody G., Colangeli L., Cooper G., Cordier P. G., Daghlian C., Dai Z., D'Hendecourt L., Djouadi Z., Dominguez G., Duxbury T., Dworkin J. P., Ebel D., Economou T. E., Fairey S. A. J., Fallon S., Ferrini G., Ferroir T., Fleckenstein H., Floss C., Flynn G., Franchi I. A., Fries M., Gainsforth Z., Gallien J. -P., Genge M., Gilles M.K., Gillet P., Gilmour J., Glavin D. P., Gounelle M., Grady M. M., Graham G. A., Grant P. G., Green S. F., Grossemy F., Grossman L., Grossman J., Guan Y., Hagiya K., Harvey R., Heck P., Herzog G. F., Hoppe P., Hörz F., Huth J., Hutcheon I. D., Ishii H., Ito M., Jacob D., Jacobsen C., Jacobsen S., Joswiak D., Kearsley A. T., Keller L., Khodja H., Kilcoyne A. L. D., Kissel J., Krot A., Langenhorst F., Lanzirotti A., Le L., Leshin L., Leitner J., Lemelle L., Leroux H., Liu M. -C., Luening K., Lyon I., MacPherson G., Marcus M. A., Marhas K., Matrajt G., Meibom A., Mennella V., Messenger K., Mikouchi T., Mostefaoui S., Nakamura T., Nakano T., Newville M., Nittler L. R., Ohnishi I., Ohsumi K., Okudaira K., Papanastassiou D. A., Palma R., Palumbo M. O., Pepin R. E., Perkins D., Perronnet M., Pianetta P., Rao W., Rietmeijer F., Robert F., Rost D., Rotundi A., Ryan R., Sandford S. A., Schwandt C. S., See T. H., Schlutter D., Sheffield-Parker J. A., Simionovici S., Sitnitsky S. I., Snead C. J., Spencer M. K., Stadermann F. J., Steele A., Stephan T., Stroud R., Susini J., Sutton S. R., Taheri M., Taylor S., Teslich N., Tomeoka K., Tomioka N., Toppani A., Trigo-Rodríguez J. M., Troadec D., Tsuchiyama A., Tuzzolino A. J., Tyliszczak T., Uesugi K., Velbel M., Vellenga J., Vicenzi E., Vincze L., Warren J., Weber I., Weisberg M., Westphal A. J., Wirick S., Wooden D., Wopenka B., Wozniakiewicz P. A., Wright I., Yabuta H., Yano H., Young E. D., Zare R. N., Zega T., Ziegler K., Zimmerman L., Zinner E., and Zolensky M. 2006. Comet 81P/Wild 2 under a microscope. *Science* 304:1711–1716.

Bunch T. E., Schultz P., Cassen P. Brownlee D. Podalak M., Lissauer J., Reynolds R., and Chang S. 1991. Are some chondrule rims formed by impact processes? Observations and experiments. *Icarus* 91:76–92.

Burchell M. J. and Kearsley A. T. 2009. Short period Jupiter family comets after Stardust. *Planetary and Space Science* 57:1146–1161.

Burchell M. J., Thomson R., and Yano H. 1999a. Capture of hypervelocity particles in aerogel: In ground laboratory and low Earth orbit. *Planetary and Space Science* 47:189–204.

Burchell M. J., Cole M. J., Lascelles S. F., Khan M. A., Barthet C., Wilson S. A., Cairns D. B., and Armes S. P. 1999b. Acceleration of conducting polymer-coated latex particles as projectiles in hypervelocity impact experiments. *Journal of Physics D (Applied Physics)* 32:1719–1728.

Burchell M. J., Cole M. J., McDonnell J. A. M., and Zarnecki J. C. 1999c. Hypervelocity impact studies using the 2 MV Van de Graaff dust accelerator and two stage light gas gun of the University of Kent at Canterbury. *Measurement Science and Technology* 10:41–50.

Burchell M. J., Creighton J. A., Cole M. J., Mann J., and Kearsley A. T. 2001. Capture of particles in hypervelocity impacts in aerogel. *Meteoritics & Planetary Science* 36:209–221.

Burchell M. J., Willis M. J., Armes S. P., Khan M. A., Percy M. J., and Perruchot C. 2002. Impact ionization experiments with low density conducting polymer based dusts as analogues of solar system dust. *Planetary and Space Science* 50:1025–1035.

Burchell M. J., Creighton J. A., and Kearsley A. T. 2004. Identification of organic particles via Raman techniques after capture in hypervelocity impacts on aerogel. *Journal of Raman Spectroscopy* 35:249–253.

Burchell M. J., Graham G., and Kearsley A. 2006a. Cosmic dust collection in aerogel. *Annual Reviews of Earth and Planetary Science* 34:385–418.

Burchell M. J., Mann J., Creighton J. A., Kearsley A. T., Graham G., and Franchi I. A. 2006b. Identification of minerals and meteoritic materials via Raman techniques after capture in hypervelocity impacts on aerogel. *Meteoritics & Planetary Science* 41:217–232.

Burchell M. J., Fairey S. A. J., Foster N. J., and Cole M. J. 2009. Hypervelocity capture of particles in aerogel: Dependence on aerogel properties. *Planetary and Space Science* 57:58–70.

Cairns D. B. 1999. Synthesis and characterisation of polypyrrole-coated latexes. Ph.D. thesis, University of Sussex, UK.

Chuang T. C., Liu Y. -C., and Wang C. -C. 2005. Improved surface-enhanced Raman scattering of polypyrrole electrodeposited on roughened substrates composed of Au–Ag bimetallic nanoparticles. *Journal of Raman Spectroscopy* 36:704–708.

Cody G. D., Ade H., Alexander C. M. O'D., Araki T., Butterworth A., Fleckenstein H., Flynn G., Gilles M. K., Jacobsen C., Kilcoyne A. L. D., Messenger K., Sandford S. A., Tyliszczak T., Westphal A. J., Wirick S., and Yabuta H. 2008. Quantitative organic and light-element analysis of comet 81P/Wild 2 particles using C-, N- and O-μ-XANES. *Meteoritics & Planetary Science* 43:353–365.

Flynn G., Bleuet P., Borg J., Bradley J. P., Brenker F., Brennan S., Bridges J. C., Brownlee D. E., Bullock E., Burghammer M., Clark B. C., Dai Z. R., Daghlian C. P., Djouadi Z., Fakra S., Ferroir T., Floss C., Franchi I. A., Gainsforth Z., Gallien J. -P., Gillet P., Grant P. G., Graham G. A., Grossemy F., Heck P., Herzog G. F., Hoppe P., Hörz F., Huth J., Igantyev K., Ishii H., Janssens K., Joswiak D., Kearsley A. T., Khodja H., Lanzirotti A., Leitner J., Lemelle L., Leroux H., Luening K., MacPherson G., Marhas K., Matrajt G., Nakamura T., Nakamura-Messenger K., Nakano T., Newville M., Papanastassiou D. A., Pianetta P., Rao W., Riekel C., Rietmeijer F., Rost D., Schwandt C. S., See T. H., Sheffield-Parker J. A., Simionovici S., Sitnitsky S. I., Snead C. J., Stadermann F. J., Stephan T., Stroud R. M., Susini J., Suzuki Y., Sutton S.R., Taylor S., Teslich N., Troadec D., Tsou P., Tsuchiyama A., Uesugi K., Vekemans B., Vicenzi E., Vincze L., Westphal A., Wozniakiewicz P. A., Zinner E., and Zolensky M. 2006. Elemental compositions of comet 81P/Wild 2 samples collected by Stardust. *Science* 314:1731–1735.

Foster N. J., Burchell M. J., Creighton A. J., and Kearsley A. T. 2007. Does capture in aerogel change carbonaceous Raman D and G bands? (abstract #1647). 38th Lunar and Planetary Science Conference. CD ROM.

Fujii S., Armes S. P., Jeans R., Devonshire R., Warren S., MacArthur S. L., Burchell M. J., Postberg F., and Srama R. 2006. Synthesis and characterization of polypyrrole-coated sulfur-rich latex particles: new synthetic mimics for sulfur-based micrometeorites. *Chemistry of Materials* 18:2758–2765.

Gies A. P., Matthew J. Vergne M. J., Rebecca L. Orndorff R. L., and Hercules D. M. 2007. MALDI-TOF/TOF CID study of polystyrene fragmentation reactions. *Macromolecules* 40: 7493–7504.

Goldsworthy B. J., Burchell M. J., Cole M. J., Armes S. P., Khan M. A., Lascelles S. F., Green S. F., McDonnell J. A. M., Srama R., and Bigger S. W. 2003. Time of flight mass spectrometry of ions in plasmas produced by hypervelocity impacts of organic and mineralogical microparticles on a cosmic dust analyser. *Astronomy & Astrophysics* 409:1151–1167.

Hörz F., Zolensky M. E., Bernhard R. P., See T. H., and Warren J. L. 2000. Impact features and projectile residues in aerogel exposed on Mir. *Icarus* 147:559–579.

Hörz F., Cintala M. J., See T. H., and Nakamura-Messenger K. 2008. Impact experiments with Al_2O_3 projectiles into aerogel (abstract 1391). 39th Lunar and Planetary Science Conference. CD-ROM.

Hörz F., Cintala M. J., See T. H., and Nakamura-Messenger K. 2009. Penetration tracks in aerogel produced by Al_2O_3 spheres. *Meteoritics & Planetary Science* 44:1243–1264.

Inoue T., Hosoya I., and Yamase T. 1987. Change of Raman scattering intensity of a polypyrrole film during reversible doping and emitting processes of ClO_4^-. *Chemistry Letters* 16:563–566.

Ishii H., Bradley J. P., Dai Z. R., Chi M., Kearsley A. T., Burchell M. J., Browning N. D., and Molster F. J. 2008. Comparison of 81P/Wild 2 dust with interplanetary dust from comets. *Science* 319:447–450.

Keaton P. W., Idzorek G. C., Rowton L. J., Seagrave J. D., Stradling G. L., Bergeson S. D., Collopy M. T., Curling H. L., McColl D. B., and Smith J. D. 1990. A hypervelocity microparticle impacts laboratory with 100 km s^{-1} projectiles. *International Journal of Impact Engineering* 10:295–308.

Keller L. P., Bajt S., Baratta G. A., Borg J., Busemann H., Brucato J., Burchell M., Colangeli L., D'Hendecourt L., Djouadi Z., Ferrini G., Flynn G., Franchi I. A., Fries M., Grady M. M., Graham G. A., Grossemy F., Kearsley A., Matrajt G., Mennell V., Nittler L., Palumbo M. E., Rotundi A., Sandford S. A., Steele A., Wooden D., Wopenka B., and Zolensky M. 2006. Infrared spectroscopy of comet Wild 2 samples returned by the Stardust mission. *Science* 314:1728–1731.

Lascelles S. F. and Armes S. P. 1995. Synthesis and characterization of micrometer-sized polypyrrole-coated polystyrene latexes. *Advanced Materials* 7:864–866.

Lascelles S. F., and Armes S. P. 1997. Synthesis and characterization of micrometre-sized, polypyrrole-coated polystyrene latexes *Journal of Material Chemistry* 7:1339–1347.

Lascelles S. F., Armes S. P., Zhdan P., Brown A. M., Greaves S. J., Leadley S. R., Watts J. F., and Luk S. Y. 1997. Surface characterization of micrometre-sized, polypyrrole-coated polystyrene latexes: verification of a 'core-shell' morphology. *Journal of Material Chemistry* 7:1349–1355.

Liu Y. C. 2004. Characteristics of vibration modes of polypyrrole on surface-enhanced Raman scattering spectra. *Journal of Electroanalytical Chemistry* 571:255–264.

McKeegan K. D., Aléon J., Bradley J., Brownlee D., Busemann H., Butterworth A., Chaussidon M., Fallon S., Floss C., Gilmour J., Gounelle M., Graham G., Guan Y. B., Heck P. R., Hoppe P., Hutcheon I.D., Huth J., Ishii H., Ito M., Jacobsen S. B., Kearsley A., Leshin L. A., Liu M. C., Lyon I., Marhas K., Marty B., Matrajt G., Meibom A., Messenger S., Mostefaoui S., Mukhopadhyay S., Nakamura-Messenger K., Nittler L., Palma R., Pepin R. O., Papanastassiou D. A., Robert F., Schlutter D., Snead C. J., Stadermann F. J., Stroud R., Tsou P., Westphal A., Young E. D., Ziegler K., Zimmermann L., and Zinner E. 2006. Isotopic compositions of cometary matter returned by Stardust. *Science* 314:1724–1728.

Neish M. J., Kitazawa Y., Noguchi T., Inoue T., Imagawa K., Goka T., and Ochi Y. 2005. Passive measurement of dust particles on the ISS using MPAC: Experiment summary, particle fluxes and chemical analysis. *Proceedings of the 4th European Conference on Space Debris*, edited by Danesy D. ESA SP-587. ESA/ESOC, Darmstadt, Germany. pp. 221–226.

Noguchi T., Nakamura T., Okudaira K., Yano H., Sugita S., and Burchell M. J. 2007. Thermal alteration of hydrated minerals during hypervelocity capture to silica aerogel at the flyby speed of STARDUST. *Meteoritics & Planetary Science* 42:357–372.

Oddi L., Capelletti R., Fieschi R., Fontana M. P., and Ruani G. 1985. New application of photocatalytic TiO_2 nanoparticles on the improved surface-enhanced Raman scattering. *Molecular Crystals and Liquid Crystals* 118:179–182.

Ormond-Prout J., Dupin D. Armes S. P., Foster N. J., and Burchell M. J. 2009. Synthesis and characterization of polypyrrole coated poly(methyl methacrylate) latex particles. *Journal of Material Chemistry* 19:1433–1442.

Perruchot C., Chehimi M. M., Delamar M., Lascelles S. F., and Armes S. P. 1996. Surface characterization of polypyrrole-coated polystyrene latex by X-ray photoelectron spectroscopy. *Langmuir* 12:3245–3251.

Roskosz M., Leroux H., and Watson H. C. 2008. Thermal history, partial preservation and sampling bias recorded by Stardust cometary grains during their capture. *Earth and Planetary Science Letters* 273:195–202.

Rotundi A., Baratta G. A., Borg J., Brucato J. R., Busemann H., Colangeli L., D'hendecourt L., Djouadi Z., Ferrini G., Franchi I. A., Fries M., Grossemy F., Keller L. P., Mennella V., Nakamura K., Nittler L. R., Palumbo M. E., Sandford S. A., Steele A., and Wopenka B. 2008. Combined micro-Raman, micro-IR and field emission scanning electron microscopy analyses of comet 81P/Wild 2 particles collected by Stardust. *Meteoritics & Planetary Science* 43:367–398.

Sandford S. A. Aléon J., Alexander C. M. O.'D., Araki T., Bajt S., Baratta G. A., Borg J., Bradley J. P., Brownlee D. E., Brucato J. R., Burchell M. J., Busemann H., Butterworth A., Clemett S. J., Cody G., Colangeli L., Cooper G., D'Hendecourt L., Djouadi Z., Dworkin J. P., Ferrini G., Fleckenstein H., Flynn G. J., Franchi I. A., Fries M., Gilles M. K., Glavin D. P., Gounelle M., Grossemy F., Jacobsen C., Keller L. P., Kilcoyne A. L. D., Leitner J., Matrajt G., Meibom A., Mennella V., Mostefaoui S., Nittler L. R., Palumbo M. E., Papanastassiou D.A., Robert F., Rotundi A., Snead C. J., Spencer M. K., Stadermann F. J., Steele A., Stephan T., Tsou P., Tyliszczak T., Westphal A. J., Wirick S., Wopenka B., Yabuta H., Zare R.N., and Zolensky M. E. 2006. Organics captured from comet 81P/Wild 2 by the Stardust spacecraft. *Science* 314:1720–1724.

Spencer M. K. and Zare R. N. 2007. Comment on "Organics captured from comet Wild 2 by the Stardust spacecraft." *Science* 317: 1680.

Spencer M. K., Clemett S. J., Sandford S. A., McKay D. S., and Zare R. N. 2009. Organic compound alteration during hypervelocity collection of carbonaceous materials in aerogel. *Meteoritics & Planetary Science* 44:15–24.

Trigo-Rodríguez J., Domínguez G., Burchell M. J., Hörz F., and Llorca J. 2008. Bulbous tracks arising from hypervelocity impact in aerogel. *Meteoritics & Planetary Science* 43:75–86.

Tsou P., Brownlee D. E., Laurance M. R., Hrubesh L., and Albee A. 1988. Intact capture of hypervelocity micrometeoroid analogs (abstract). 19th Lunar and Planetary Science Conference. pp. 1205–1206.

Tsou P., Brownlee D. E., Sandford S. A., Hörz F., and Zolensky M. E. 2003. Wild 2 and interstellar sample collection and Earth return. *Journal of Geophysical Research* 108(E10); 8113, doi: 1029/2003/JE002109.

Zolensky M. E., Zega T. J., Yano H., Wirick S., Westphal A. J., Weisberg M. K., Weber I., Warren J. L., Velbel M. A.,

Tsuchiyama A., Tsou P., Toppani A., Tomioka N., Tomeoka K., Teslich N., Taheri M., Susini J., Stroud R., Stephan T., Stadermann F. J., Snead C. J., Simon S. B., Simionovici A., See T. H., Robert F., Rietmeijer F. J. M., Rao W., Perronnet M. C., Papanastassiou D. A., Okudaira K., Ohsumi K., Ohnishi I., Nakamura-Messenger K., Nakamura T., Mostefaoui S., Mikouchi T., Meibom A., Matrajt G., Marcus M. A., Leroux H., Lemelle L., Le L., Lanzirotti A., Langenhorst F., Krot A. N., Keller L. P., Kearsley A. T., Joswiak D., Jacob D., Ishii H., Harvey R., Hagiya K., Grossman L., Grossman J. N., Graham G. A., Gounelle M., Gillet P., Genge M. J., Flynn G., Ferroir T., Fallon S., Ebel D. S., Dai Z. R., Cordier P., Clark B., Chi M., Butterworth A. L., Brownlee D. E., Bridges J. C., Brennan S., Brearley A., Bradley J. P., Bleuet P., Bland P. A., Bastien R. 2006. Mineralogy and petrology of comet Wild 2 nucleus samples. *Science* 314:1735–1739.